New Condensed Cluster Structure with Triple Metal Layers: La_2INi_2 and La_2ICu_2. Synthesis, Structure, and Bonding

Seung-Tae Hong, James D. Martin, and John D. Corbett*

Department of Chemistry, Iowa State University, Ames, Iowa 50011

Received January 30, 1998

Syntheses of the title compounds result from appropriate reactions of the elements and LaI_3 in sealed Nb or Ta containers at 800 °C. These exhibit a new structural type with an unusual metal-rich layered structure, detailed for La_2INi_2 by single-crystal X-ray diffraction: hexagonal $P\bar{6}m2$, $Z = 1$, $a = 4.1387$ Å, $c = 8.814$ Å (23 °C). This is related to the Gd_2IFe_2-type structure known for La_2IZ_2 for Z = Fe, Co, and others. Both structures contain AlB_2-like slabs, namely, graphite-like Z_2 (Z = Ni, Fe) layers between eclipsed pairs of La layers, but these are instead separated by single iodine layers. The La_2INi_2 structure differs in that the iodine positions along $\vec{c}$ project onto only one Z position instead of both and the cell is half as large. An additional set of very weak reflections and streaks revealed in widely varying amounts by precession photographs suggests a superstructure in *c* or intergrowths by small amounts of disordered components, but a reasonable model could not be derived beyond some possible short-range disordering in the iodine layers. Comparisons of La_2INi_2 with La_2IFe_2 in terms of electronic band structures show that filling of antibonding states occurs in the Ni layers. Integrated overlap populations in the Fe vs Ni compounds show corresponding decreases for Z−Z and La−Z bonding and a smaller strengthening of La−La bonding in the layers, while the *a* lattice parameter increases and the trigonal prismatic La_6Z units decrease in height. These conflicts are reflected in the Z-layer puckering and the doubled *c* dimension found in La_2IFe_2 and other phases with the Gd_2IFe_2-type structure.

Introduction

Well-reduced rare earth metal (R) halide systems exhibit an exceedingly prolific and diverse cadre of novel compounds based on octahedral R_6X_{12}-type clusters.[1−3] Their most remarkable feature is that these exist, with very few exceptions, only when stoichiometric amounts of a third element, Z, act as interstitial stabilizers. Although the last are known to include the main-group elements H, B−N, Si, etc., the most versatile and useful Z have come from among the late transition metals in all three periods, viz., Mn−Cu, Ru−Pd and Re−Au. The beautiful structural varieties found among these phases start with isolated clusters and different halogen-interbridging modes, all of these being relatively well reduced because of the electron-poor characteristic of the R elements, e.g., in $R_7X_{12}Z$, $R_6X_{10}Z$, and $R_{12}X_{17}Z_2$[4] stoichiometries. The chemistry also extends to condensed varieties in which octahedral-type clusters share metal edges to form chains in monoclinic Pr_4I_5Ru,[5] double chains in monoclinic Pr_3I_3Ru,[6] and a three-dimensional condensate in the cubic polytype Pr_3I_3Os.[7] With further reduction, compounds form in which Z layers centered between double metal layers are interleaved with double and then by only single halogen layers, the latter in Gd_2IFe_2[8,9] and R_2XZ,[10,11] for instance.

A series of lanthanum iodide examples with the Gd_2IFe_2-type structure have been found for Z = Fe, Co, Ru, or Os,[12] but the powder diffraction patterns obtained at the same time for the Ni and Cu compounds showed a related but unknown hexagonal (or trigonal) structure with ∼*a* and *c*/2 dimensions. Recently, single crystals of La_2INi_2 have been obtained, and the new structure type revealed. The present article describes the new structure as well as weak evidence for a superstructure that is evidently caused by short-range disordering of iodine. A comparison and discussion is provided regarding La_2INi_2 vs La_2IFe_2 (Gd_2IFe_2-type) structures in terms of electronic band calculations and the derived orbital populations as these influence structural and bonding changes in phases with this unusual layer stacking sequence (I−La−Z_2−La).

Experimental Section

Syntheses. The general reaction techniques in welded $^3/_8$-in. o.d. Nb or Ta tubing jacketed by sealed, fused silica containers, the use of Guinier powder photography for both phase identification and approximate yield estimates, and the crystallographic characterization

(1) Corbett, J. D. *J. Alloys Compd.* **1995**, 229, 10.
(2) Corbett, J. D. In *Modern Perspectives in Inorganic Crystal Chemistry*; E. Parthé, Ed.; Kluwer Academic Press: Dordrecht, 1992; pp 27−56.
(3) Simon, A.; Mattausch, Hj.; Miller, G. J.; Bauhofer, W.; Kremer, R. K. *Handbook on the Physics and Chemistry of Rare Earth*; Gschneidner, K. A., Eyring, L., Eds.; Elsevier Science Publishers: Amsterdam, Netherlands, 1991; Vol. 15, p 191.
(4) Park, Y.; Corbett, J. D. *Inorg. Chem.* **1994**, *33*, 1705.
(5) Payne, M. W.; Dorhout, P. K.; Corbett, J. D. *Inorg. Chem.* **1991,** *30*, 1467.
(6) Payne, M. W.; Dorhout, P. K.; Kim, S.-J.; Hughbanks, T. R.; Corbett, J. D. *Inorg. Chem.* **1992,** *31*, 1389.
(7) Dorhout, P. K.; Payne, M. W.; Corbett, J. D. *Inorg. Chem.* **1991**, *30*, 4960.
(8) Ruck, M.; Simon, A. *Z. Anorg. Allg. Chem.* **1993,** *619*, 327.
(9) Ruck, M., Ph.D. Dissertation, University of Stuttgart, 1991.
(10) Bauhofer, C.; Mattausch, Hj.; Miller, G. J.; Bauhofer, W.; Kremer, R. K.; Simon, A. *J. Less-Common Met.* **1990,** 167, 65.
(11) Martin, J. D.; Corbett, J. D., unpublished research.
(12) Park, Y.; Martin, J. D.; Corbett, J. D. *J. Solid State Chem.* **1997**, *129*, 277.

S0020-1669(98)00119-0 CCC: $15.00
Published on Web 06/11/1998

Table 1. Lattice Constants (Å) and Cell Volumes (Å^3) of R_2IZ_2 Phases[a]

	a	*c*	*V*	*c/a*
La_2INi_2[b]	4.1387(9)	8.814(2) [17.628(4)]	130.75(9) [261.5(2)]	[4.259]
La_2ICu_2[b]	4.250(1)	8.667(1) [17.333(2)]	135.57(8) [271.1(2)]	[4.078]
La_2IFe_2[c,d]	4.116(2)	18.121(8)	265.9(4)	4.403
La_2ICo_2[d]	4.0883(9)	17.899(4)	259.1(2)	4.378
La_2IRu_2[d]	4.2996(7)	17.820(7)	285.3(2)	4.145
La_2IRh_2[d]	4.119(1)	17.65(2)	259.3(4)	
La_2IOs_2[d]	4.2995(4)	17.972(5)	287.7(1)	
Pr_2INi_2[d]	4.083(2)	17.211(2)	248.5(3)	4.215
Gd_2IFe_2[e]	4.0143(5)	17.180(2)	239.76(9)	
Gd_2ICo_2[e]	3.9830(5)	17.036(1)	234.06(7)	

[a] From Guinier powder diffraction data with Si as internal standard, λ=1.54 056 Å, 22 °C. [b] $P\bar{6}m2$ (this work); the 2*c*, 2*V*, and 2(*c*/*a*) values are listed in brackets for comparison. [c] This and subsequent compounds are Gd_2IFe_2-type, $P6_3/mmc$. [d] Ref 12. [e] Ref 8.

means have been described before.[4,5,12] All reactants and products were handled only in a N_2-filled glovebox (H_2O < 0.1 ppm vol). The reagents La metal (Ames Lab), sublimed LaI_3 (prepared from the elements), and powdered Ni and Cu metals (Johnson-Matthey, ≥99.9% metal purity) were utilized on 200−300 mg reaction scales. The La_2IZ_2 (Z = Ni, Cu) phases came from reactions of LaI_3 with the appropriate amounts of the elements at 800 °C for 4 weeks. Yields were 80−90%, with LaOI as the only other detectable compound, the oxygen probably originating with the H_2O evolved from silica jacket with time.

X-ray Studies. An Enraf-Nonius (FR-552) Guinier camera was used for phase identifications and lattice constant determinations. Protection of the samples between layers of cellophane tape has been described earlier.[13] Powdered standard silicon (NIST) was included with each sample in order to provide an internal calibration scale for the film. Lattice constants of each phase were then obtained by standard least-squares refinement of measured and indexed reflections in its pattern. The lattice parameter results for La_2IZ_2 (Z = Ni, Cu) synthesized in this course of research are listed in Table 1 along with those for Z = Fe, Co, Ru, Rh, Os[12] and for Gd_2IZ_2 (Z = Fe, Co)[8] for later comparison. It is to be noted that no reflections with *l* = odd for the larger Gd_2IFe_2 cell could be found in any of the Guinier powder X-ray patterns of the two new lanthanum phases. Weak evidence for a doubled cell in *c* was detected in precession photos of single crystals secured with Ni-filtered Cu radiation over very long exposure times (several days). It should be noted that these (*h*0*l*), (0*kl*), and (*hhl*) photographs also showed weak continuous streaks through the spots and parallel to [001], indicating some appreciable disordering of atoms along $\vec{c}$. Some crystals yielded only strong streaks without giving discernible superstructure spots, indicating even greater disordering in those. Accordingly, all powder patterns showed unusually diffuse lines. The larger cell was later identified during automatic tuning procedures on the diffractometer for about half of the many crystals examined. Powder patterns calculated for the normal cells of the two new compounds according to the structural solution for the nickel phase agreed very well with the observed patterns in both line positions and intensities.

Diffraction data were collected at room temperature on a single-crystal diffractometer (Rigaku AFC6R) for the doubled supercell over a sphere of reciprocal space (2θ < 50°) from a 0.10 mm × 0.09 mm × 0.06 mm La_2INi_2 crystal sealed in a thin-walled glass capillary. Data for the normal cell were reduced in order to solve and refine the basic structure since ordinary least-squares refinements of the superstructure had not been successful. The data for the regular cell exhibited no extinction conditions, which indicated possible hexagonal space groups $P\bar{6}m2$, $P\bar{6}$, $P6/mmm$, $P\bar{6}2m$, $P6mm$, $P622$, $P6/m$, and $P6$ (R_{av} ($I > 3\sigma_I$) = 4.1%). However, space groups with 6 or with *m* symmetry operations parallel to (100) could be easily disregarded since too-close contacts between I or La atoms (depending on the origin) are unavoidable with these symmetries and for this type of structure. This leaves the acentric space groups $P\bar{6}m2$ and $P\bar{6}$, which are also consistent with the N(Z) test on intensity statistics. Both gave statistically the same crystal structure, so the higher symmetry $P\bar{6}m2$ was chosen. Absorption was first corrected with the aid of the average of three ψ-scans. Direct methods[14] were used for the structure solution. The remainder of the refinement was entirely routine.[15] Application of DIFABS after isotropic refinement of ψ-scan-corrected data, as recommended,[16] improved the absorption correction (μ = 288.97 cm^{-1}) by giving more nearly isotropic displacement ellipsoids. Finally, the enantiometric configuration was refined for comparison. The final residuals were $R(F)/R_w$ = 1.8/2.0%. The largest residuals in the final ΔF map were +0.6 e$^-$/Å^2 1.0 Å from La and −0.4 e$^-$/Å^3 0.2 Å from La. Some data collection and refinement parameters are given in Table 2, while more details are given in the Supporting Information. These and the corresponding F_o/F_c data are also available from JDC. The final atom coordinates and isotropic equivalent temperature factors and their standard deviations are listed in Table 3 together with important bond distances.

Table 2. Data Collection and Refinement Parameters for La_2INi_2

formula weight	522.10
crystal system, space group, *Z*	hexagonal, $P\bar{6}m2$ (no. 187), 1
lattice constants[a]	
a (Å)	4.1387(9)
c (Å)	8.814(2)
V (Å^3)	130.75 (9)
d_{calc} (g/cm^3)	6.63
temperature (°C)	23
μ (Mo Kα, cm^{-1})	288.97
R, R_w,[b] %	1.82, 1.96

[a] From Guinier powder data with Si as internal standard, λ = 1.54 056 Å, 23 °C. [b] $R = \sum||F_o| - |F_c||/\sum|F_o|$; $R_w = [\sum w(|F_o| - |F_c|)^2/\sum w(F_o)^2]^{1/2}$; $w = \sigma_{F^{-2}}$.

Table 3. Atomic Positional Parameters and Important Distances (Å) in La_2INi_2

atom	*x*	*y*	*z*	U_{iso}[a]
La	0	0	0.2876(1)	0.0147(7)
I	1/3	2/3	0	0.0150(1)
Ni1	2/3	1/3	1/2	0.0221(2)
Ni2	1/3	2/3	1/2	0.0163(2)

distances

La−La		3.744(3), 4.1387(9)[b]
Ni−Ni	× 3	2.3895(6), 4.1387(9)[b]
La−I	× 3	3.4843(9)
La−Ni	× 6	3.0353(9)
I−I		4.1387(9)[b]

[a] $U_{iso} = {}^1/_3\sum_i\sum_j U_{ij}a_i^*a_j^*\bar{a}_i\bar{a}_j$. [b] The *a*, *b* axial repeats.

What turned out to be a final and futile attempt to define a single structure for a 2*c* supercell started with the evidence that could be obtained by Fourier mapping. Observed independent reflections ($I > 3\sigma_I$) for the regular subcell numbered 117 out of 122 possible, with ($I_{max}/\sigma_I > 87$). In contrast, the supposed supercell-unique (*l* = odd) data set contained only ~111 out of 1814 measured data ($I > 0$), and only 26 of the independent reflections had $I > 3\sigma_I$, with the largest $I_{max}/\sigma_I = 9$. Since the superstructure data were few and weak, the superstructure was supposed to be a slight modification of the substructure. But the odd-*l* data were not adequate in number and intensity to allow successful least-squares refinement of any model because of disastrous coupling. A Fourier map was then computed with the total data set and suitably transformed atom parameters from the refined regular subcell. It is to be noted that only the odd-*l* reflections allow a distinction of the superstructure from the substructure, but the phases of these cannot be correctly obtained from the normal cell expansion because all of their magnitudes are zero. Thus, a slight perturbation from the ideal structure was needed to get nonzero

(13) Daake, R. L.; Corbett, J. D. *Inorg. Chem.* **1978,** *17*, 1192.

(14) Sheldrick, G. M. SHELXS-86, Universität Göttingen, Germany, 1986.

(15) Watkin, D. J.; Prout, C. K.; Carruthers, J. R.; Betteridge, P. W. *CRYSTALS, Issue 10*; Chemical Crystallography Laboratory, University of Oxford: Oxford, UK, 1996.

(16) Walker, N.; Stuart, D. *Acta Crystallogr.* **1983**, *A39*, 158.

F_{calc} for odd-*l* and corresponding meaningful phases. Many small perturbations of the positional parameters of La or Ni or of the occupancies of any atom resulted in basically the same map. Even so, the Fourier map (Supporting Information) was flat to a level of ~4.5 $e^-/Å^3$ except for input atoms, while one computed with only odd-*l* data was relatively meaningless. The ΔF map for all data suggested a possible superstructure model in which a small fraction of iodine atoms was disordered in alternate positions within the iodine layer, but there were also small unexplainable electron densities which in part may have arisen from errors in the odd-*l* data (below). (It was later found that the nature of the displacements used to achieve a useful ΔF map also changed that result significantly.) A trial model with a minor fraction of disordered iodine was therefore adopted for the superstructure, as could result from an intergrowth of a Gd_2IFe_2-like component. Atom positions and, eventually, anisotropic parameters and the occupancies were refined by least-squares methods using strong restraints[17] on the changes per cycle and with the thermal parameters of the distinct lanthanum and iodines in the supercell constrained to be the same. Eventually this yielded (23 variables, 143 reflections) converged residuals of $R/R_w = 8.3/7.2\%$. However, the model at this point was unbelievable, the added disordered iodine position having grown to a size that was inconsistent with the weakness of the odd-*l* reflections. Presumably, this originated with large and systematic errors in the odd-*l* data set, the intensities of which reflected only the somewhat more preferred 2*c* repeats along diffraction streaks that actually represented a wide distribution of other distances. Some small disordering of the iodine positions in its layer is the limit of explanation that seems possible according to the meager information available about the doubled cell.

Band Calculations.[18] Three-dimensional, tight-binding band calculations on La_2INi_2 and La_2IFe_2 were carried out at 216K points. For La_2IFe_2, the fractional coordinates of Gd_2IFe_2 were used,[8] but these were also modified a little so that *d*(La−I) was equal to that in La_2INi_2 and/or the Fe slabs were not puckered. However, calculations with these modifications did not show any significant changes in DOS, COOP, or total energy results. The standard (default) H_{ii} parameters (eV) were used for La (5d, −8.21; 6s, −7.67; 6p, −5.01)[19] while those for Ni (3d, −12.404; 4s, −8.125; 4p, −4.184), Fe (3d, −10.822; 4s, −7.659; 4p, −4.104), and I (5s, −21.069; 5p, −11.561) came from density functional theory.[20] The orbital exponents employed were the standard default values in the Cornell program.

Results and Discussion

Crystal Structure. The new phases La_2INi_2 and La_2ICu_2 adopt a new structural type ($P\bar{6}m2$) for double metal layered halides containing interstitials. At the beginning of this study, some modification of the Gd_2IFe_2-type ($P6_3/mmc$) structure of La_2IZ_2 (Z = Fe, Co, Ru, Rh, Os) was thought to apply to La_2IZ_2 (Z = Ni, Cu) phases since their powder X-ray diffraction patterns were rather similar. However, no reflections for $l =$ odd could be detected, although these are fairly strong in the former structure. In fact, very weak odd-*l* reflections were observed but only on precession films or by a directed search on the single-crystal diffractometer. Therefore, the basic cell La_2IZ_2 (Z = Ni, Cu) must be only slightly modified in any ~2*c* supercell component (below).

The unique crystal structure of La_2INi_2 was solved and refined from single-crystal data (Experimental Section). Figures 1 and 2 show views of the La_2INi_2 structure normal and parallel to the unique *c* axis; these views are in the opposite sense parallel and normal to the (La−Ni−La−I) layering sequence, respectively. The triple metal layers contain Ni in all trigonal prismatic

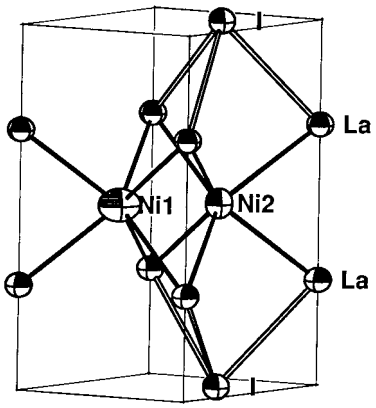

Figure 1. Off-[110] view of one cell of La_2INi_2 (90% probability).

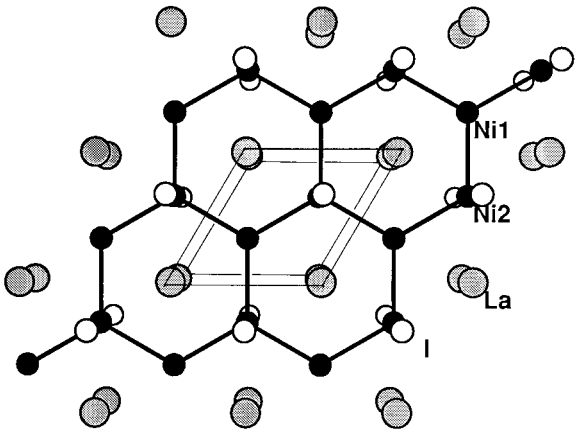

Figure 2. ~[001] view of La_2INi_2. Ni atoms (solid) within a slab are connected. The La atoms are gray, and I atoms are open circles.

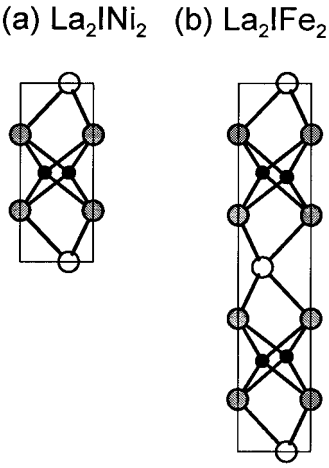

Figure 3. [110] sections of (a) La_2INi_2 and (b) La_2IFe_2 (Gd_2IFe_2-type) structures. The origin in the latter has been shifted by *c*/4 for a clearer comparison. The La atoms are shaded, I atoms are open, and Ni or Fe atoms are solid circles.

cavities between pairs of eclipsed (but internally close-packed) La layers (Figure 2). This disposition generates graphite-like Ni layers with short Ni−Ni distances, $a/\sqrt{3} = 2.384$ Å. Figure 3 compares the (110) sections of the cells of (a) La_2INi_2 and (b) La_2IFe_2 (Gd_2IFe_2 type). The AlB_2 structure type contains the same three-layer arrangement as do the metal layers in $(La_2Ni_2)I$ and $(La_2Fe_2)I$, but here these are not co-condensed but separated by single iodine layers. The main difference between La_2INi_2 and Gd_2IFe_2 comes from the iodine positions which project along $\vec{c}$ onto only one Z position and onto alternate Z positions, respectively, the latter thus giving zigzag iodine

(17) Watkin, D. J. *Acta Crystallogr.* **1994**, *A50*, 41.
(18) Whangbo, M. H.; Hoffmann, R.; Woodward, R. B. *Proc. R. Soc. London* **1979,** A366, 23.
(19) Zheng, C.; Hoffmann, R., unpublished results.
(20) Vela, A.; Gázquez, J. L. *J. Phys. Chem.* **1988**, *92*, 5688.

ordering along a doubled *c* axis. Accordingly, the layering sequence for La(Ni)$_2$La**I** is (A(bc)A**C**) rather than (A(bc)A**B)**(A-(bc)A**C)** for Gd(Fe)$_2$Gd**I**, La(Fe)$_2$La**I**, etc. the latter also have a slightly puckered Z slab in parallel with the iodine placement.

Superstructure. Precession photographs of (*h*0*l*), (0*kl*), and (*hhl*) nets from several La_2INi_2 single crystals revealed very weak odd-*l* reflections, suggesting a *c* dimension close to that for the Gd_2IFe_2-type structure for La_2IFe_2. All of the small number of extra reflections ($\leq$26 with $I/\sigma_I > 3$) lay on streaks of varying intensity along $\vec{c}$, which for some crystals, obscured the coherent scattering altogether. Structure factor calculations for sets such as (*h*0*l*) showed that odd-*l* intensities for the La_2IFe_2 structure are determined mostly by the zigzag iodine ordering along *c* (Figure 3b), and these are quite strong and easily observed in the powder pattern. Small displacements of atoms (e.g., Z-layer puckering) contribute very little; thus, any hints of a La_2INi_2 superstructure must originate with only slight displacements or disordering of some atoms relative to the predominant subcell.

As expected, direct structural solutions from supercell data in various possible space groups (e.g., $P\bar{6}m2$, $P\bar{6}$, even $P\bar{3}$, $P3$, etc.) gave statistically the same structure as the subcell one, and all failed in the later stages of the least-squares fit refinement owing to high correlations between temperature factors of La and I atoms that formerly were in single sites. The only clear indication of a small difference in any supercell came from a Fourier map. This suggested that a small amount of electron density lay in the alternate iodine position at $z = {}^1/_2$, indicating an effective disordering of iodine. However, this could not be refined to any sensible result (see Experimental Section) perhaps because of the inevitable poor quality of the odd-*l* intensity data, i.e., from systematic losses of diffraction intensity into streaks along $\vec{c}$. Thus, these hints of a 2*c* cell may result from intergrowths of a Gd_2IFe_2 structure type into La_2INi_2, but there are many other distributions as well, judging from the range of streaking encountered in precession photographs of different crystals, even from the same preparation.

Extended Hückel Band Calculations. A significant question about the series of La_2IZ_2 (Z = Fe−Cu) is why do Fe and Co compounds *adopt* the Gd_2IFe_2-type structure, while Ni and Cu *occur* in another type? The answer appears to do with both electronic structure and size. To understand more about the nature of the bonding interactions in these structure types, extended Hückel band calculations have been performed on La_2INi_2 and La_2IFe_2. The total densities-of-states for the Ni and Fe phases are shown in Figure 4, with the La contributions projected out in each. Most of iodine 5p contributions fall in the range of −13 to −12 eV, while Z (Ni or Fe) provides most of the remaining contributions above there. Metallic conductivity is clearly expected for both phases. It also appears that these band structure results can be regarded approximately in a rigid band sense.

Figure 5 provides further clarification through the COOP curves (overlap-weighted atom-pair populations) as a function of energy for all La−Z, La−I, La−La (both parallel and normal to *a*), and Z−Z interactions. (Although the abscissa scales are the same for each compound, the COOP curves for different atom pairs in each cannot be compared precisely because of the different overlap integrals incorporated.) Band energy calculations for imaginary structures, that is, for La_2INi_2 with La_2IFe_2 structure and vice versa, showed no significant differences in DOS and COOP results from those for the actual structures. This implies that energy differences originating with the zigzag ordering of iodine in projection and/or the Z-layer puckering are too small to have an appreciable effect at this level of calculation, though they may be important for the real structures. Direct I−I interactions across the slabs (>8 Å) are too long to be responsible for the ordering difference.

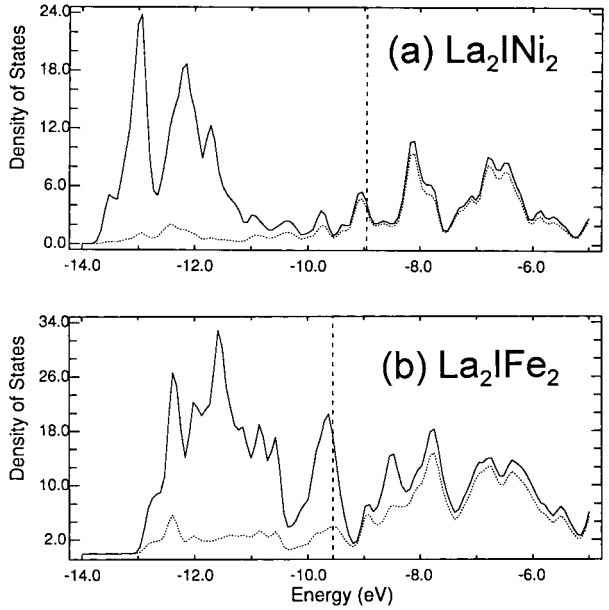

Figure 4. The densities-of-states for (a) La_2INi_2 and (b) La_2IFe_2. The projection of lanthanum contributions are defined by the dotted line. Iodine 5p constitutes most of the remaining contribution in the range of −13 to −12 eV, and Z (Fe, Ni), at higher energies.

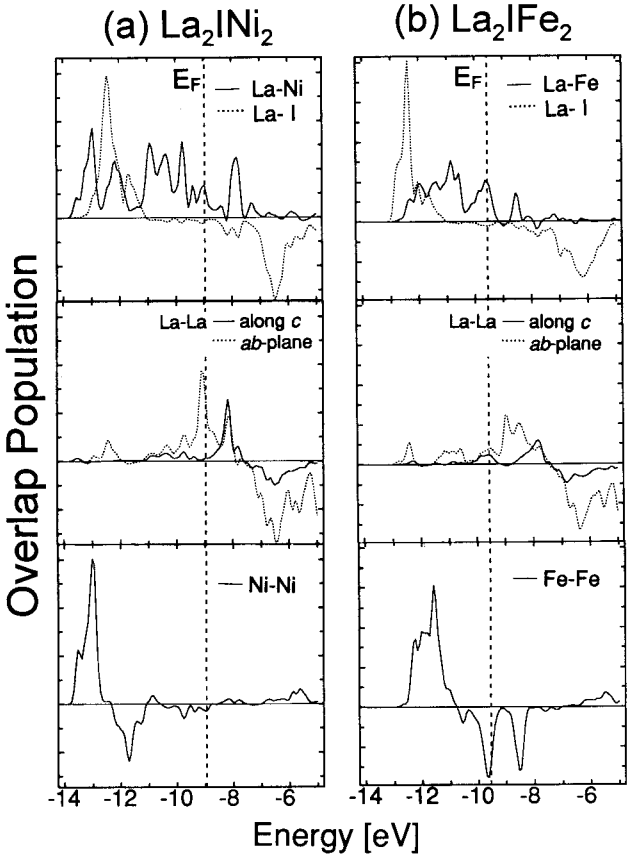

Figure 5. COOP curves vs energy for various interactions for (a) La_2INi_2 and (b) La_2IFe_2: La−Z, La−I, La−La along *c*, La−La parallel to the *a*−*b* plane, and Z−Z. Overlaps out to 4.2 Å are included. The overlap population scale is the same for each compound.

Table 4. Integrated Overlap Populations for La_2INi_2 and La_2IFe_2 with Comparable Electron Counts (Rigid Band)[a]

	La_2INi_2	$La_2INi_2 - 4e^-$	La_2IFe_2	$La_2IFe_2 + 4e^-$
Z−Z	0.342	0.427	0.795	0.517
La−Z	1.76	1.10	2.31	2.60
La−I	1.17	1.22	1.21	1.18
La−La($\vec{c}$)	0.111	0.034	0.075	0.100
La−La($\vec{a}$)	0.601	0.129	0.311	0.676

[a] Per formula unit. The Gd_2IFe_2 atom coordinates have been adjusted to give reasonable La−I distances in La_2IFe_2.

The major bonding contributions in these layer structures seem to be the strong mixing of La 5d with both I 5p and Z 3d that are evident in both compounds, Figure 5, while La−La bonding appears less important. However, differences in Z−Z bonding between La_2INi_2 and La_2IFe_2 are clear from the COOP curves; the former has most of the Ni−Ni antibonding bands filled, while Fe−Fe bonding is evident in the latter, although this too becomes unfavorable near E_F. In both cases, net Z−Z bonding contributes much less than La-Z and La−I bonding in term of overlap populations. Metal−metal bonding between later transition metals always has more antibonding states filled because of their electron-richer nature. Integrated overlap populations for the various bond types per formula unit given in Table 4 make these effects clearer, data being listed for both the indicated compounds and the rigid band result with the appropriate change of ±4 electrons. This makes it clearer that there is a weakening of Z−Z but a moderate strengthening of La−Z and La−La bonding within the slabs with an increased number of electrons according to both calculations. The La−I bonding contributions remain fairly constant throughout.

Puckering of the Z Slab. The principal points distinguishing the La_2IFe_2 and La_2INi_2 structures are the iodine ordering and Z-slab puckering, and these are strongly correlated with each other. Suppose the Ni layers were to pucker to any extent for some reason; then, one iodine atom would be closer to Ni than the other, and the symmetry of the identical iodines (bottom and top of Figure 1a) would be broken. Symmetry would require a zigzag iodine ordering and a Gd_2IFe_2-type structure (or other), even though the energy difference might be very small. Conversely, the latter iodine ordering would also cause Z-slab puckering, but because of the long I−I interactions across the slab, we presume a puckered Z layer causes the iodine ordering rather than the other way round. Then the question is, Why are the Z slabs puckered? In this connection, it should be noted that the La−Z distance, d(La−Z), is much more affected by Z-layer puckering than is d(Z−Z). Geometrically, puckering of the Fe layer by ±0.10 Å (as in Gd_2IFe_2) changes d(Fe−Fe) by not more than 0.01 Å but changes d(La−Fe) by about ±0.07 Å. In other words, puckering is an easy way to adjust d(La−Z) without any significant change in d(Z−Z).

Structural Choice. The respective space groups reflect the fact that the centrosymmetric La_2IFe_2 has only a single type of Fe atom in a puckered layer, while the acentric group of La_2INi_2 requires two nonequivalent Ni atoms to describe what must be a high symmetry planar Z sheet. We surmise that this phase may be of marginal stability thermodynamically under our experimental conditions since the products always had what might be interpreted as an intergrowth of Gd_2IFe_2-type (or higher) repeats into La_2INi_2 and in widely varying degrees. However, if one focuses on just the triple metal La−Z−La slabs, the trigonal prismatic ZLa_6 site in La_2INi_2 has the higher symmetry, with six equivalent La−Z bonds, while La_2IFe_2 exhibits two La−Fe bond lengths because of the puckered Z layer.

Dimensional changes through the series La_2IZ_2 for Z = Fe−Cu and Pr_2INi_2 (Table 1, ref 12) are especially informative and supportive of previous conclusions. Standard Z−Z bond lengths ($2R_{12}$ or $2R_1$, Pauling[21]) slowly decrease by ∼0.02 Å per step in the series Fe−Co−Ni but then increase by 0.04 Å at Cu. The c lattice dimensions observed for La_2IZ_2 decrease regularly over the same Z. On the other hand, a decreases from Fe (4.116 Å) to Co (4.088 Å) then turns up moderately for Ni (4.139 Å) and markedly for Cu (4.250 Å). These reflect the combined effects of the size of metal Z and the strengths of the Z−Z bonds in a rigid band sense. The size effect is responsible for the change between Fe and Co, while for Ni, the electronic change is predominant. For Cu, both are responsible. The comparable cell volumes of La_2IZ_2 parallel the latter changes. (A striking volume increase at Cu has also been seen across the late 3d elements in the electron-rich interstitial hosts La_5Ge_3Z and Zr_5Pb_3Z.[22,23]) In contrast, c/a ratios are close for Fe and Co and appreciably lower for Ni and Cu (Table 1); that is, the La_6 trigonal prisms are distinctly taller in the doubled cell (∼0.2 Å in d(La−La)). The remainders of the cell heights (the La−I−La sequence) remain nearly constant to reflect constant d(La−I). These can be understood in terms of the strengths of La−Z and La−La. There are two ways of making a shorter average $\bar{d}$(La−Z), a smaller a-parameter or a shorter La−La distance along c. The former will reduce the Z−Z as well as horizontal La−La distances, but the a parameter appears to be affected more by Z−Z bonding and the size of Z. Thus, for a given a parameter, $\bar{d}$(La−Z) is mostly determined by La−La along c; that is, a stronger La−Z bond will induce a shorter La−La distance along c for a heavier Z, consistent with the observations.

The interlayer d(La−La) and average $\bar{d}$(La−Fe) distances would be 3.965 and 3.096 Å, respectively, in an unpuckered La_2IFe_2 structure with the same a axis if d(La−I) (3.434 Å) were instead comparable to that in La_2INi_2, 3.484 Å. However, this 3.096 Å value for $\bar{d}$(La−Fe) would be distinctly (0.061 Å) longer than d(La−Ni), 3.035 Å, in contrast to a difference of only ∼0.016 Å in standard metallic radii. However, puckering of Fe slabs (by, say, ±0.10 Å) would generate three shorter and more suitable distances (3.026 Å) plus three longer (3.165 Å) La−Fe bonds in the taller trigonal prism observed. A three-short, three-long bonding scheme is more stable than that of six mid-length La−Fe for any system with an exponential dependence of bond length on order. On the other hand, the stronger La−Ni and La−La bonding induce a La−La distance along $\vec{c}$ (3.744 Å) that is much less than those found in reduced lanthanum cluster halides. In this case, the lanthanum to nonpuckered Ni distance (3.035 Å) is already short enough for six equivalent La−Ni bonds. Puckering in this system would give a too small d(La−Ni) value, obviously not favorable.

A similar result is obtained when Pr is substituted for La in R_2INi_2. Both axes decrease because of the smaller R, and c/a remains nearly the same. However, the decreases in a, 0.056 Å, is less than expected for the difference in metallic R diameters, 0.094 Å, suggesting that the contraction has been limited and the Z layer is again found puckered.[12] The 0.032 Å decrease in d(Ni−Ni) from that in $LaINi_2$ is also accompanied by a 0.036(3) Å difference in the two d(Pr−Ni).

(21) Pauling, L. *The Nature of the Chemical Bond*; Cornell University Press: Ithaca, NY, 1960; p. 400.
(22) Guloy, A. M.; Corbett, J. D. *Inorg. Chem.* **1993**, *32*, 3532−3540.
(23) Kwon, Y.-U.; Corbett, J. D. *J. Alloys Compd.* **1993**, *190*, 219−227.

Acknowledgment. S.-T.H. gratefully acknowledges Dr. D.-K. Seo for many helpful discussions pertaining to the interpretation of the EHBC. This research was supported by the National Science Foundation, Solid State Chemistry, via Grants DMR-9207361 and -9510278 and was carried out in the facilities of the Ames Laboratory, U.S. Department of Energy.

Supporting Information Available: Two tables listing more crystallographic data and the anisotropic thermal ellipsoids plus a Fourier map (3 pages). Ordering information is given on any current masthead page.

IC980119X